Nuclear Materials and Energy 9 (2016) 153–156

Contents lists available at ScienceDirect

Nuclear Materials and Energy

journal homepage: www.elsevier.com/locate/nme

Melt-layer formation on PFMs and the consequences for the material performance

I. Steudel*, A. Huber, A. Kreter, J. Linke, G. Sergienko, B. Unterberg, M. Wirtz

Forschungszentrum Jülich GmbH, Institut für Energie- und Klimaforschung, 52425 Jülich, Germany

ARTICLE INFO

Article history:
Available online 4 August 2016

ABSTRACT

One of the numerous challenges of the demonstration power plant DEMO is the selection of appropriate plasma facing materials (PFMs) and this task is ultimately important to the success for DEMO. Low-activation stainless steel (e.g. EUROFER, P92), which is already intended as structural material, could also become a possible plasma facing material, e.g. for the first wall (FW). Therefore, the ferritic martensitic steel P92 was investigated under DEMO relevant loading conditions. An area of the sample surfaces was firstly molten by transient events with varying power densities (A = 245 MW/m^2, B = 708 MW/m^2) and afterwards simultaneously and sequentially exposed to thermal and particle loads. Surface modifications and pronounced microstructure changes were investigated dependent on the pre-exposure, loading sequence and power density. More precisely, it turned out that there was no connection between the loading sequence and the surface modifications for the preloaded A-samples contrary to preloaded B-samples. The preloaded B-samples exhibited surface roughening, melting and the formation of holes dependent on the loading sequence and power density.

1. Introduction

The environmental conditions in DEMO for the in-vessel components and thus for the armour materials are severe and complex [1,2]. The PFMs must not only withstand steady state heat loads, edge localised modes (ELMs) but also off-normal events (disruptions, “hot” and “cold” vertical displacement events (VDEs)), runaway electrons (RE), high particle and neutron fluxes [3,4]. Tungsten is still a main candidate as PFM but also ferritic-martensitic steels, which are foreseen as structural material in DEMO, could become contingent candidates for PFMs [4]. Therefore, more research is needed. However, the present comprehensive experiments investigated several exposure parameters at once, to predict the performance of the ferritic-martensitic steel P92. The experiments were executed in two test devices, the electron beam facility JUDITH 1 [5] and the linear plasma generator PSI-2 [6]. JUDITH 1 was used to melt the surfaces by transient thermal events. Afterwards, the preloaded samples were exposed to thermal (Nd: YAG laser) and particle (deuterium plasma) loads in the linear plasma generator PSI-2. Furthermore, the exposure sequences were varied. This work focuses on the influence of melt layer formation/solidification and sequential/simultaneous loading on the damage behaviour of stainless steel, changes of the morphology, and consequential risks regarding the application.

2. Experimental

The industrially available, ferritic martensitic steel P92 (X10CrWMoVNb9-2, BGH Edelstahl Freital GmbH) was investigated. Samples with the dimensions $12 \times 12 \times 5$ mm^3 were cut from the round blank and afterwards polished to a mirror finish to obtain a well-defined surface structure. The first part of the experiments, with the purpose to create solidified surfaces, was realised in the electron beam facility JUDITH 1, located at Forschungszentrum Jülich. The electron beam was used to simulate transient events with different power densities that could affect the FW in DEMO and could cause melting. For the A tests, a power density of 245 MW/m^2 (corresponding to a heat flux factor $F_{HF} \sim 13$ MW/m^{2}s$^{0.5}$) was used to ensure melting. Different pulse numbers (10, 100 and 1000) were applied with a pulse duration of 3 ms to an area of 8×8 mm^2. The B tests were done at a power density of 708 MW/m^2 (corresponding to a $F_{HF} \sim 22$ MW/m^{2}s$^{0.5}$) and with varying pulse numbers of 10 and 100. Furthermore, the pulse duration was 1 ms and the exposed area had to be downscaled to 6×6 mm^2 to achieve the intended loading conditions. All electron beam experiments were done at room temperature (RT) and with loading parameters that guaranteed the melting of

* Corresponding author.
E-mail address: i.steudel@fz-juelich.de (I. Steudel).

http://dx.doi.org/10.1016/j.nme.2016.08.002

Table 1
Overview of the loading conditions of tests in JUDITH 1 (preloading) and PSI-2.

Preloading	A-sample	B-sample	Loading PSI-2	Pre. A-sample	Pre. B-sample
Loaded area [mm^2]	8 × 8	6 × 6	Preloading pulse number	1000	100
Pulse duration [ms]	3	1	Pulse duration [ms]	1	1
Pulse number	10/100/1000	10/100	Repetition frequency [Hz]	0.5	0.5
Power density [MW/m^2]	245	708	Pulse number	100/1000	100/1000
F_{HF} [MW/m^{2}s$^{0.5}$]	13	22	Power density [GW/m^2]	0.16–0.66	0.16–0.66
Base temperature [°C]	RT	RT	Base temperature [°C]	400	400
			Loading sequence	1–4	1–3
	Loading sequence	1. laser (100) → plasma	2. plasma + laser (100)	3. plasma → laser (100)	4. plasma → laser (1000)

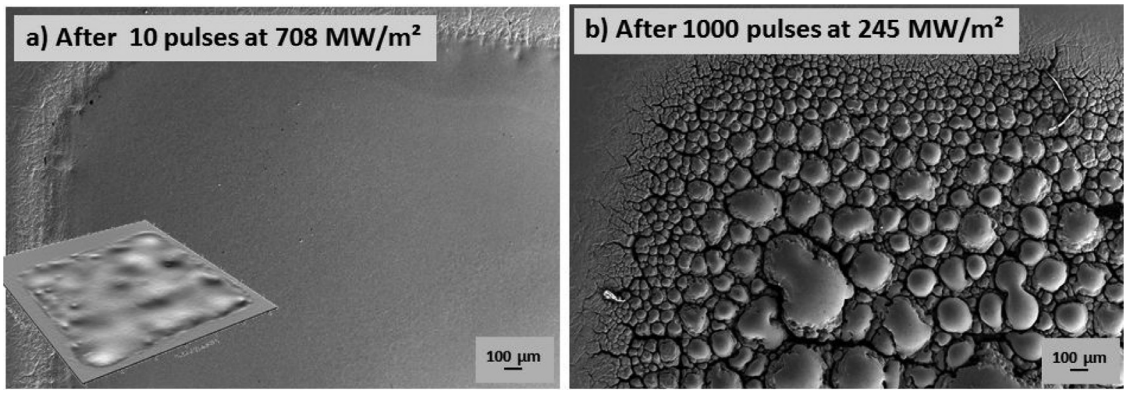

Fig. 1. Surface morphology after exposure in JUDITH 1. a) shows the surface after 10 pulses at 708 MW/m^2. The profilometer scan displays clearer the wavy structure. b) shows a surface after 1000 pulses at 245 MW/m^2 which caused a pronounced hill-valley structure.

the surface [7]. Afterwards, the samples were investigated by laser profilometry and scanning electron microscopy (SEM). The second part of the tests was the sequential and simultaneous exposure to thermal and particle loads at the linear plasma device PSI-2, where the power density and plasma parameters were retained but the order of loading and the pulse number were changed. Therefore, the preloaded targets were mechanically clamped to a holder and heated to a base temperature of 400 °C. During the tests, a Nd: YAG laser with a wave length of $\lambda = 1064$ nm and a maximum energy of 32 J was used for the thermal shock events with a repetition frequency of 0.5 Hz and a pulse duration of 1 ms. The applied power densities covered a range of 0.16 – 0.66 GW/m^2. The particle exposure was realised by pure deuterium plasma with a flux of $\sim 6 \cdot 10^{21}$ m^{-2} s^{-1} and a fluence of up to $\sim 1.2 \cdot 10^{25}$ m^{-2} (corresponding to 1000 laser pulses). In addition, a bias voltage of 60 V accelerated the particles towards the sample which resulted in an ion energy of 35 eV. After the cessation, the preloaded A-samples held four exposure spots while the preloaded B-samples held three due to the smaller solidified area. In detail, the first spot was primarily exposed to 100 transient thermal events and subsequently to plasma. On the second spot, the loading was simultaneous, while the third and fourth (only for preloaded A-samples) spots were initially loaded with plasma followed by 100/1000 thermal pulses, respectively. Afterwards, the induced damages and surface modifications were analysed by light microscopy, SEM and metallographic cross sections. Table 1 summarises all loading conditions to give a better overview.

3. Results and discussion

Fig. 1 illustrates exemplarily a sample surface after 10 events at 708 MW/m^2 (1a) and after 1000 events at 245 MW/m^2 (1b). It became apparent that the A-samples, which were exposed at 245 MW/m^2, experienced greater surface modifications and ended up with pronounced hill-valley morphologies. This effect intensified with increasing the applied pulse number and was driven by the occurrence of melt layers and their motion due to cohesive forces. After 100 pulses at 708 MW/m^2 the loaded area showed a smooth, wavy surface in comparison to the A-samples, which were loaded at 245 MW/m^2. These uneven surface modifications seem to be affected by the different pulse numbers, pulse durations and power densities/F_{HF}. Especially, the different F_{HF}, stainless steel will start melting at $F_{HF} \sim 13$ MW/m^{-2}s$^{0.5}$ [8], in combination with the varying pulse numbers influenced the surface modification massively.

However, for the following tests in PSI-2, the samples with the heaviest marked surface modifications were used, to investigate the worst case. As mentioned before, due to the larger area on preloaded A-samples, four spots with different loading sequence could be applied. Fig. 2 shows the different exposure spots for different power densities based on SEM images in the top row and metallographic cross sections in the bottom row. By direct comparison, the surface modifications are independent of the loading sequence. Furthermore, only some isolated cracks were found in the valleys, most of the cracks originated in the hills either due to the rapid cool down after each pulse or due to hydrogen accumulation that also generates stresses and drives embrittlement.

Additionally, the cross section images showed the single interfaces between the different phases which had formed during the melt cycles. Also, cavities were detected in the hills which could be a result of the repeated shallow surface melting followed by a fast solidification or an effect of the cross section preparation. However, cavities could decrease the connection to the bulk material and could lead to thermal barriers, a risk for overheating and melting. Another observation was that the small hills grew together to big hills due to the repetitive melting and this became more distinct with an increase of the applied power density as well as the pulse number.

Different from the preloaded A-samples, the analysis of the preloaded B-samples revealed a clear influence of the exposure sequence on the surface modifications. Fig. 3 displays this influence by SEM and metallographic cross section images after experiments

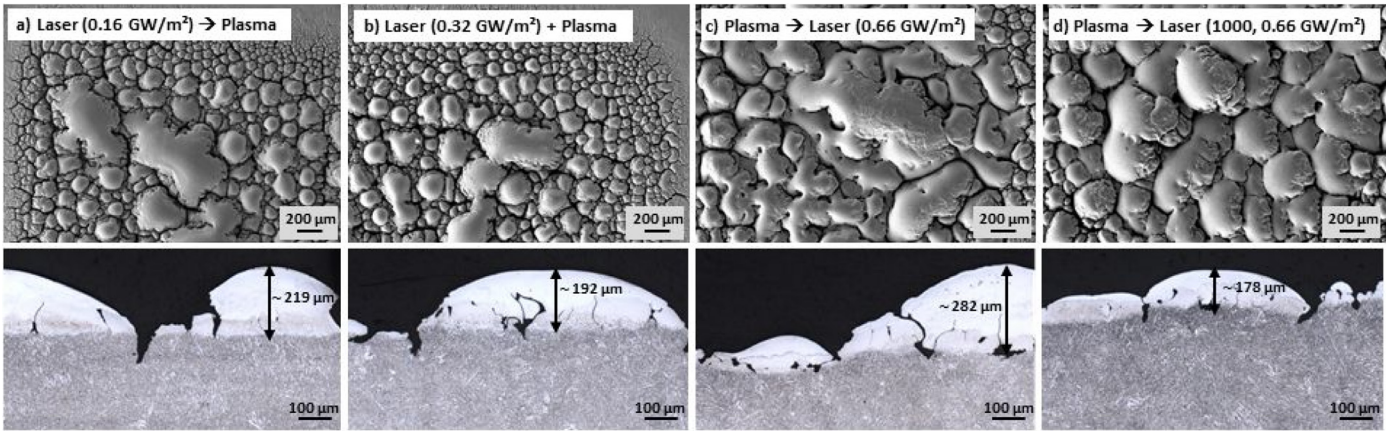

Fig. 2. Preloaded A-sample after exposure in PSI-2. The top row shows SEM images of the loaded spots with varying sequences and power densities starting with the lowest power density in image a) and ending with the highest power density(and pulse number) in d). The bottom row illustrates the related metallographic cross sections.

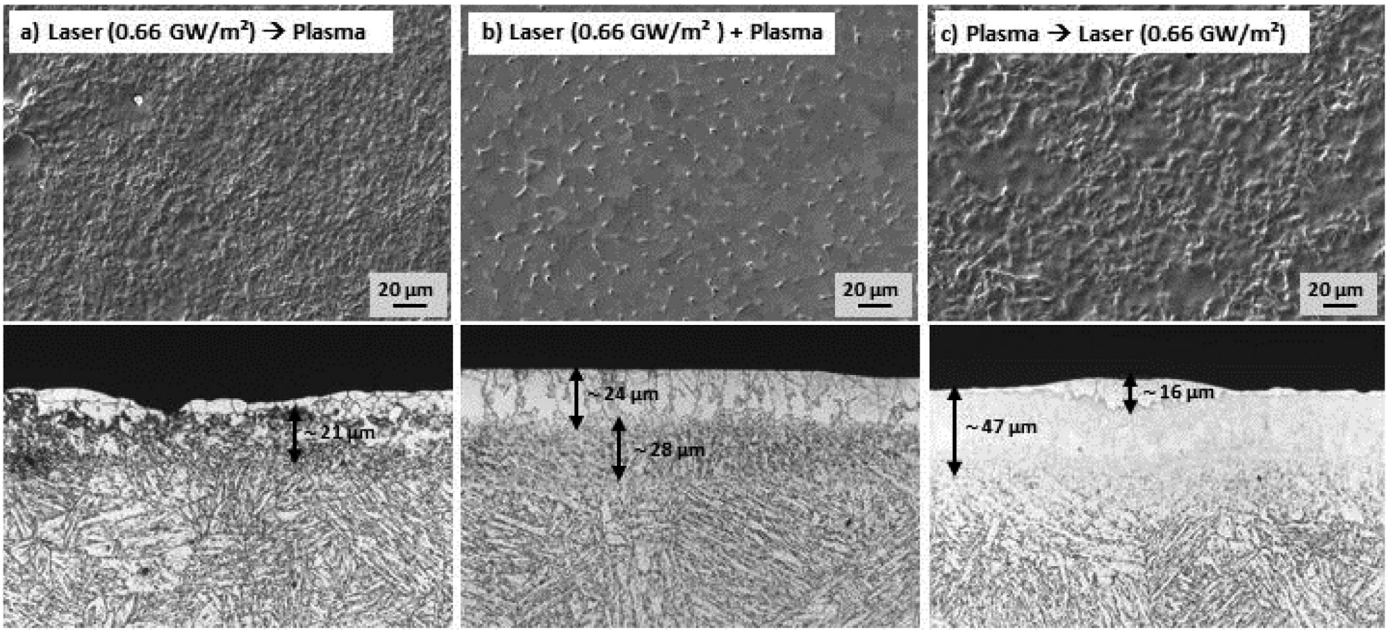

Fig. 3. Representative SEM images (top row) and metallographic cross section images (bottom row) of a preloaded B-sample after sequential and simultaneous experiments at the highest power density. The influence of the loading sequence is mirrored in the surface modifications that can be seen in the top row.

at the highest applied power density (0.66 GW/m^2). Investigating the first exposure spot (Fig. 3a top row), which first saw 100 laser pulses and subsequently the deuterium plasma, the surface roughness increased from $R_a = 0.35\,\mu m$ (arithmetic mean roughness R_a after electron beam exposure) up to $R_a = 1.2\,\mu m$. This increase was accompanied by partial molten parts of the preloaded surface and small cracks that originated in the near surface region. The small cracks were observed for each sequence at the lowest power density of 0.16 GW/m^2. For power densities above 0.16 GW/m^2 small cracks were also detected but without an obvious relation to the loading sequence. Furthermore, simultaneous exposure at 0.66 GW/m^2 led to small holes on the surface which can be seen in Fig. 3b top row. These holes were evenly distributed over the entire loaded area and frequently at the point where several grains encounter each other.

Taking the epitaxial grain growth at the near surface region into account the grain boundaries are straight and perpendicular to the surface so that this could be the preferential and easiest way for the hydrogen to interact with the material. An assumption is that outgassing and/or accumulation of hydrogen accompanied by the arising stresses leads to the observed material loss and formation of holes. However, further investigations, e.g. retention measurements, focused ion beam cross sections, need to be performed to get revealing and instructive results. The loading sequence that started with plasma exposure followed by 100 laser pulses induced stresses that led to plastic deformation and therefore an increase of the surface roughness as well as molten parts at the exposed area those were more numerous and marked compared against the reverse order. In conclusion, the observed differences of the surface morphology are not only arising due to the order of exposure also due to the applied power density.

4. Conclusions

The experiments, combining melting and the creation of solidified surfaces with sequential and simultaneous thermal and particle exposure showed that the kind of preloading influences the surface morphology significantly and this surface morphology again influences the performance and damage behaviour. The results of the electron beam tests exhibited that with increasing the

pulse number for tests with the smaller F_{HF} (A-samples), the sample surfaces evolved a pronounced hill-valley structure. For the B-samples, which were tested at the higher F_{HF}, the specimens ended up with smoother wavy surfaces which could be reasoned by the complete cool down between two batched pulses, the lower amount of pulses and the higher F_{HF} that could have caused complete melting of the loaded area. In conclusion, the electron beam experiments caused severe melting, formation of melt-layers, and melt motion and further experiments are needed and planed, e.g. the preloading of A-samples and B-samples with the same pulse number, to draw well-grounded conclusions about the parameters responsible for the changes in the surface morphology.

The second part of this experiment, the sequential and simultaneous exposure to thermal and particle loads, brought out that the sequential loading had no effect on the preloaded A-samples. Furthermore, only the applied power density as well as pulse number showed an influence on the surface modification. This influence was observed by the merging of separate hills to one hill due to successive melting. The preloaded B-samples acted entirely different. In detail, the loading sequence had a significant impact on the surface modification and damage behaviour that became more distinct with an increase of the power density. The surface roughness increased conspicuously accompanied by partially molten parts for sequences that started or ended with laser exposure, whereby the sequence ending with laser exposure generated the higher surface roughness and amount of molten parts. An explanation could be the stresses in the material, generated by the thermal shocks and the hydrogen concentration in the near surface region, which led to plastic deformation. Moreover, this plastic deformation was more distinct because ending with laser exposure implies that at the beginning of the sequence the amount of hydrogen in the near surface region was higher than for the sequence vice versa. Regarding the operation of DEMO this conspicuous surface roughness increase indicates that fatigue effects could appear faster in the case of distinct higher pulse numbers and therefore the risk of crack formation, origination of thermal barriers and melting would increase [9]. All these things would shorten the lifetime of the in-vessel components and/or negatively influence the frictionless operation of DEMO. Another observation was that simultaneous exposure created small holes all over the entire loaded area. An assumption could be that the outgassing of hydrogen led to material loss accompanied by plastic deformation. To make a valid statement about this observation and to understand the underlying processes further investigations are planed like focused ion beam cross sections and retention measurements.

To further support this conclusions, following experiments will aim on better comparable, initial conditions for the electron beam tests. In addition, to characterise the synergistic effects of steady state hydrogen exposure and thermal shock exposure and to identify important threshold values and material parameters the exposure parameters have to be expand.

References

[1] H. Bolt, et al., J. Nucl. Mater. 307–311 (2002) 43–52.
[2] D Stork, et al., Fusion Eng. Des. 89 (2014) 1586–1594.
[3] Yu Igitkhanov, et al., J. Nucl. Mater. 438 (2013) 440–444.
[4] N. Baluc, Nucl. Fusion 47 (2007) S696.
[5] M. Rödig.et al., J. Nucl. Mater. Part 1, 53-59 (2002), 307–311
[6] A Kreter, et al., Fusion Sci. Technol. 68 (2015) 8–14.
[7] I Steudel, et al., J. Nucl. Mater. 463 (2015) 731–734.
[8] N.S Klimov, et al., J. Nucl. Mater. 438 (2013) 241–245.
[9] Th Loewenhoff, et al., Fusion Eng. Des. 87 (2012) 1201–1205.